18th International Conference on Space Operations, Montreal, Canada, 26 - 30 May 2025.

SpaceOps-2025, ID # 417

Cosmic Ray mitigation for Euclid's Fine Guidance Sensor

Frederic Schmidt [a]

[a] *Telespazio Germany GmbH, Europaplatz 5,64293 Darmstadt Germany*, *frederic.schmidt@telespazio.de*

Abstract

The European Space Agency's (ESA) EUCLID space-based optical/near-infrared survey mission was launched on 1st of July 2023 to investigate the nature of dark matter, dark energy and gravity by observing the geometry of the Universe and the formation of structures over cosmological timescales. EUCLID requires very precise attitude control with very high pointing accuracy, which is achieved by using the Fine Guidance Sensor (FGS). The FGS is equipped with four CCDs that image the sky from the sides of the 'field of view' of Euclid's VISible instrument (VIS). The sensor uses guide stars from the GAIA catalogue to navigate and feeds this data into the spacecraft's Attitude and Orbit Control System (AOCS) to orient and maintain the telescope's precise pointing. During the commissioning phase it became apparent that cosmic rays were causing false signals to be identified as real stars on the CCD sensor during the acquisition phase, resulting in the inability to resolve the correct star patterns needed for navigation. The FGS application software has been enhanced by the manufacturer LEONARDO with a double image filter algorithm that allows the identification and rejection of false targets caused by cosmic rays. This paper describes the FGS operational concept, the mitigation of cosmic rays during the FGS acquisition phase, the enhancements to the AOCS application software and the FGS performance improvements.
Keywords: Euclid, Fine Guidance Sensor, GAIA catalogue, Cosmic Ray

Nomenclature

This section is not numbered. A nomenclature section could be provided when there are mathematical symbols in your paper. Superscripts and subscripts must be listed separately. Nomenclature definitions should not appear again in the text.

Acronyms/Abbreviations

Attitude and Orbit Control System (AOCS)
Acquisition Phase (AP)
Application SoftWare (ASW)
Absolute Tracking Mode (ATM)
Acquisition Phase of the Absolute Tracking Mode (ATM-TP)
Coarse Mode of the Absolute Tracking Mode (ATM-CM)
Fine Mode of the Absolute Tracking Mode (ATM-FM)
Intermediate Cycle of the Absolute Tracking Mode (ATM-IC)
Tracking Phase of the Absolute Tracking Mode (ATM-TP)
Background (BKG)
Basic SoftWare (BSW)
Charge Coupled Device (CCD)
Electrically Erasable Programmable Read-Only Memory (EEPROM)
European Space Agency (ESA)
Electronic Unit (EU)
FGS On board catalogue Generation tool (FOG)
Field Of View (FOV)
Field-Programmable Gate Array (FPGA)
Fine Guidance Sensor (FGS)
Focal Plan Assembly (FPA)
HardWare (HW)
Intermediate Cycle (IC)
Line Of Sight (LoS)
On Board Catalogue (OBC)
On-Ground Algorithm (OGA)

Proximity Electronic Channel (PEC)
Proximity Electronic Modules (PEM)
Processing Module (PM)
SpaceCraft (SC)
Standby Mode (SBM)
SpaceWire (SpW)
Thales Alenia Space Italy (TASI)
Telecommand (TC)
Telemetry (TM)
Tracking Phase (TP)
VISible instrument (VIS)

1. Introduction

The first sections provides an overview of the EUCLID mission followed by an introduction to the architecture, design, software and different modes of the Fine Guidance Sensor (FGS) used on the ESA astronomy mission EUCLID. Section 4 addresses the in-flight observations seen during the first FGS commissioning and their mitigations. In Section 5 the in-flight results taken from the second FGS recommissioning using the new double image correlator algorithm are presented.

2. Euclid mission overview

Euclid is a space-based optical/near-infrared survey mission of the European Space Agency (ESA) to investigate the nature of dark energy, dark matter and gravity by observing the geometry of the Universe and on the formation of structures over cosmological timescales [1,2]. Euclid will use two probes of the signature of dark matter and energy: Weak gravitational Lensing, which requires the measurement of the shape and photometric redshifts of distant galaxies, and Galaxy Clustering, based on the measurement of the 3-dimensional distribution of galaxies through their spectroscopic redshifts. The mission was launched on 1st of July in 2023 and is designed for 6 years of nominal survey operations. The Euclid Spacecraft is composed of a Service Module and a Payload Module. The Service Module comprises all the conventional spacecraft subsystems, the instruments warm electronics units, the sun shield and the solar arrays. In particular the Service Module provides the extremely challenging pointing accuracy required by the scientific objectives. The Payload Module consists of a 1.2 m three-mirror Korsch type telescope and of two instruments, the visible imager and the near-infrared spectro-photometer, both covering a large common field-of-view enabling to survey more than 35% of the entire sky. All sensor data are downlinked using K-band transmission and processed by a dedicated ground segment for science data processing. The Euclid data and catalogues will be made available to the public at the ESA Science Data Centre [2].

3. Euclid Fine Guidance Sensor

3.1 Fine Guidance Sensor architecture

The Fine Guidance Sensor (FGS) is the one of the core elements of the Euclid AOCS that allows the compliance to the stringent pointing requirements of the mission by measuring the telescope line-of sight direction with ultra-high accuracy. To perform its task, the sensitive parts of the FGS need to be placed as close as possible to the VIS focal plane to minimise differential optical-thermo-elastic deformation and maintain the FGS LoS as stable as possible with respect to the VIS channel LoS. The location of the FGS detectors shall permit FGS measurements during VIS readout (which is performed after the closure of the VIS shutter). The implementation of the FGS requires an extension of the FoV on each side of the Focal Plane Assembly (FPA) in the optical path direction (see Fig. 1). In this configuration the FGS and VIS focal plane and readout electronics are coupled not only from a mechanical and optical point of view, but also from a thermal and shall limit the potential thermal and EMC disturbances to the VIS FPA due to FGS high frequency readout [3].
The FPA architecture consists of 2 CCD detectors and 1 plate support built in SiC. The FPA and Proximity Electronics Module (PEM) are electrically connected through the CCD flex, but mechanically decoupled. In order not to induce noise on the VIS readout channel and to stop the thermal flux towards the focal plane, two EMI shields and two thermal shields are placed between the PEM and the FPA
To achieve the required accuracy, two detectors on opposite sides (see Fig. 1) of the focal plane X-axis shall be operating at the same time; the allowed CCD pairs are (R1,L1), (R2,L2), (R1,L2) and (R2,L1).

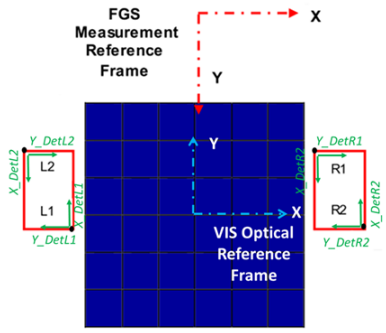

Fig. 1 VIS and FGS focal plane with respect to Payload Module reference frame

The Fine Guidance Sensor architecture comprises three functional elements (Focal Plane Assembly, FPA; Proximity Electronics Module, PEM; Electronic Unit, EU) implemented as five separated items (FPA-left, FPA-right, PEM-left, PEM-right, EU), linked together by dedicated harnesses, as shown in the schematic diagram of Fig. 2. Each FPA is composed of two CCD detectors, a mechanical structure and the harness (realized with flexible PCBs) to connect each CCD to the relevant Proximity Electronic Channel. Each PEM includes 2 identical channels (Proximity Electronic Channel - PEC), each interfacing a CCD detector with a size of 4096 by 4096 pixels. The PEM and FPA pairs are mounted in the PLM, on either side of the VIS FPA (Fig. 2). The EU is placed in the SVM directly connected to the satellite CDMU and PCDU. The EU performs management of the complete FGS. It is internally redundant and connected to the 4 PECs in order to improve the FGS system reliability [3].

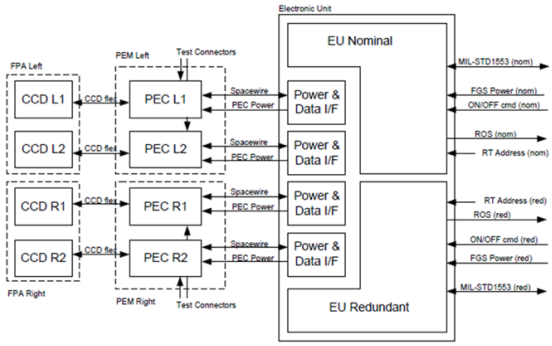

Fig. 2 FGS schematic

3.1 FGS Software and modes

3.1.1 FGS Software

The FGS Eelectronic Unit EU executes the FGS Basic and Application software.

The Basic Software (BSW), includes:

- Start-Up Software (SUSW), which implements the start-up code and the maintenance modes of the FGS. It resides on dedicated boot EEPROMs, not writable in flight. The SUSW first performs the initial set-up and check of the instrument, except the PECs that are maintained switched off (this part is executed directly from the EEPROM), then the SUSW code is uploaded in RAM and the FGS is synchronized with the CDMU, via the 1553 milbus and protocol [3].

- Hardware-Dependent Software (HDSW), which provides services and a static library for the Application Software.

The Application Software (ASW) implements the operational modes of the FGS. The ASW resides in dedicated EEPROM and is loaded in RAM and launched by dedicated TC by the SUSW. The ASW can manage all the low level HW items by means of the HDSW interaction.

ASW and SUSW are never working at the same time, even if part of the SUSW will remain resident in RAM to allow a “soft” re-boot, in which the second phase of the SUSW is directly executed. The SUSW and the ASW constitute the FGS OBSW.

A SpaceWire interface is implemented to send commands to the PECs and receive the related pixel data (raw and processed by the FPGA). The FGS provides also a digital signal to inform about errors occurred during startup (Report Of Startup - ROS) before milbus communication is available.

3.1.2 FGS operating modes

The FGS operating modes and mode transitions are illustrated in Fig. 3. Modes are implemented in both SUSW and ASW. The FGS implements two modes supporting the AOCS science mode, with and without use of an onboard star catalogue: Relative Tracking Mode (RTM) and Absolute Tracking Mode (ATM). The FGS basic cycle while tracking is 0.5 Hz, therefore 1 fresh measurement each 2 seconds is provided. The 2 second cycle allows a longer exposure time (up to 1.5s) increasing therefore the collected signal, while the noise is basically constant. In the presented paper only the Absolute Tracking mode, which uses the onboard star catalogue, will be presented since it is the main FGS mode to support science observations.

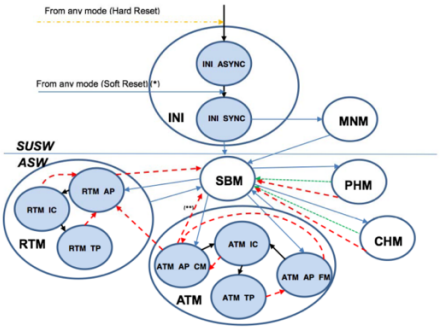

Fig. 3 FGS mode transition diagram

3.1.3 FGS Absolute Tracking Mode

This mode is started after reception of devoted telecommand, indicating the CCDs to be used for the attitude determination. ATM consists of three main phases, Acquisition Phase (ATM-AP) used for attitude initialisation, Intermediate Cycle (ATM-IC), which is needed to cope with star displacement occurring between acquisition and tracking phase and Tracking Phase (ATM-TP) used for attitude tracking.

In ATM the star catalogue is used. The star catalogue is the On Board Catalogue file (OBC) used in every pointing to find the stars to be tracked. It is collecting all the information to be transmitted to the FGS. The content of this file is a merge of other output files produced by the On ground algorithm (OGA), which uses the GAIA star catalogue as input. The OBC is composed of a triad catalogue with spherical angle values, used for absolute pattern recognition, and a list of up to 80 stars per CCD, which can be used in ATM-TP. A triad is a triplet of stars including a main star *i* and two secondary stars *j* and k. A triad is characterized by the spherical angle between stars *j* and *k*, with respect to *j* and *i*, the Angular distance between stars *i* and *j*, the Angular distance between stars *i* and *k*, the Magnitude of the three stars and the index of the three stars. The catalogue includes, for each star, a flag including star classification and desirability, that can be exploited by the ASW target selection algorithms [5].

The mode's output consists of an absolute quaternion relative to the Inertial Reference Frame and a relative attitude quaternion with respect to the initially validated and locked quaternion, similar to the RTM.
It is important to note that the primary goal of the FGS is to enhance the attitude stability by minimizing the Relative Pointing Error, even in ATM mode. Therefore, in ATM, star selection is performed with the objective of reducing relative pointing error, prioritizing the brightest stars for attitude computation.
To further enhance the accuracy of the measured absolute quaternion, only a subset of the brightest tracked objects—those with a catalog position knowledge error below a specified threshold—are used in the computation. This is contingent on the availability of a sufficient number of stars meeting the criteria. The measured angular rate is also calculated and provided in telemetry.

Attitude initialisation can be performed in two ways:

- Initialisation for large attitude uncertainties (90 arcsec 3sigma or +/- 900 pixels (22% of CCD area)) – coarse mode
- Initialisation for low attitude uncertainties (5 arcsec 3sigma or +/- 100 pixels (5% of CCD area)) – fine mode

In ATM-AP, the FGS receives an estimation of the current absolute quaternion evaluated by the star tracker. Depending on the on-board attitude knowledge error, FGS attitude initialization can be performed in Coarse Mode (for large attitude uncertainties <90 arcsec 3σ) or Fine Mode (for small attitude uncertainties <5 arcsec 3σ).

If the a priori attitude uncertainty is low, the FGS performs initial acquisition directly in windows mode using enlarged windows (50×50 pixels). The window positions are determined based on the initial quaternion estimate and the star catalogue, allowing attitude initialization to be completed within 3 seconds.

For high attitude uncertainty, the FGS performs a full CCD readout and executes a pattern recognition algorithm to identify detected stars. To improve efficiency, the algorithm can use a predicted attitude as input to limit the number of stars considered during star matching and to perform congruence checks. The full ATM-AP process takes per first design 6 seconds.

In both cases, target selection considers the position on the CCD, the star's magnitude, and the estimated position accuracy provided in the star catalogue.

The Intermediate Cycle (ATM-IC) is conducted to account for star displacement and adjust the window size accordingly. During ATM-IC, attitude and angular rate calculations are performed and validated against expected values, while stars and windows are selected for the Tracking Phase. To accommodate star displacement uncertainty, enlarged windows of 50×50 pixels may be used. The entire process takes 3 seconds.

In ATM-TP (Tracking Phase), the FGS acquires images in window mode with a variable exposure time ranging from 0.1s to 1.5s at a frequency of 0.5Hz, followed by the readout of CCD data. For each target window, after clustering the targets, a selection procedure is applied, taking into account the magnitude and distance of the targets. Up to 10 selected targets per CCD are used for the attitude measurement. Detected targets are compared with a hot-pixel lookup table, and any target whose cluster contains a hot pixel is discarded for that cycle [5]. Only the validated targets from both active CCDs are used for attitude calculation, and if multiple valid targets are found within a tracking window, they are resolved and both star data are used for the measurement.

ATM-TP provides the attitude of the FGS reference frame relative to the Inertial Reference Frame (IRF). During this phase, the FGS propagates the stars validated during the intermediate cycle to continue tracking the same stars. If a star exits the field of view (due to a slew), it is replaced with a new star based on the expected positions derived from the onboard catalogue and the measured inertial attitude. The AOCS then begins using the attitude measured by the FGS at the first valid Tracking Phase cycle, which is when the attitude is locked.

4. In-Flight Observations and Mitigations for FGS Acquisition Phase

During the FGS commissioning activities after launch, a reduced capability to successfully complete the Acquisition Phase (AP) was observed in-flight compared to expectations [6]. This issue was more pronounced in fields of view (FoV) with medium or low star densities, approximately 50 stars per FoV and 10 stars per FoV, respectively.
Two main factors contributed to this reduced AP success rate:

- **Presence of Cosmic Rays (CRs):** CR impacts created star-like clusters that could not be effectively filtered by the FGS.
- **Reduced Star Signal:** The stars produced a weaker-than-expected signal, affecting their detectability.

To address these challenges, two key modifications were studied, implemented, and successfully tested in-flight during re-commissioning:

- **Double Image Correlator Algorithm:** This algorithm was introduced to distinguish persistent targets (i.e., stars) from randomly occurring cosmic ray impacts. Two consecutive full-frame image acquisitions are performed under identical conditions (same exposure time, RLE threshold, and binning). Detected clusters in the second image are cross-checked with the first image; only those clusters that match are validated, while the others are discarded. Since true stars maintain consistent position and magnitude across both acquisitions, whereas cosmic rays appear randomly with varying brightness, this approach significantly improves CR rejection.
- **Increased Exposure Time:** The exposure time during the pattern recognition phase was increased from 1.5 seconds to 3.5 seconds. This adjustment compensates for the reduced star signal, restoring the detectability of dim stars to match the initial design specifications.

4.1 Double image correlator algorithm performance evaluation

The performance of the double image correlator algorithm was assessed through simulations. LEONARDO developed a MATLAB model of the algorithm, which generated and post-processed two full-frame pixel images with binning, containing both stars and cosmic rays (CRs) [7]. The number of stars, their magnitude range, and the number of CRs were configurable inputs.

To account for star measurement errors, slight variations were introduced in the positions and magnitudes of the stars between the two images. A position error of 0.3 pixels (1 sigma) and a magnitude error of 0.2 magnitude (1 sigma) were considered. Both stars and CRs were uniformly distributed across the images, with CRs randomly selected from an ESA-provided library containing 310,694 entries [7].

Fig. 4 illustrates the magnitude distribution of CRs in the ESA library, showing that most CRs have magnitudes between 15 and 17, making them bright and easily detectable by the FGS. Further analysis of the ESA CR library confirms that the shape of CRs closely resembles that of stars (see Fig. 5 and Fig. 6), with a median size of 5 pixels and a median length of 3 pixels. Due to this similarity, many CRs cannot be effectively filtered out using the cluster filter algorithm alone. To improve cosmic ray rejection and enhance AP success, the implementation of the new double image correlation algorithm was necessary.

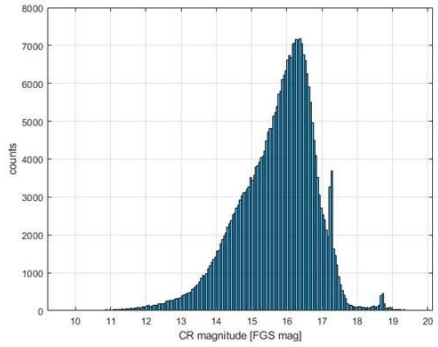

Fig. 4 Magnitude distribution for cosmic rays [7]

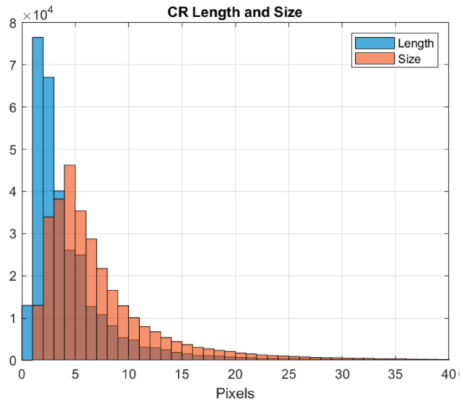

Fig. 5 Cosmic ray length and size [7]

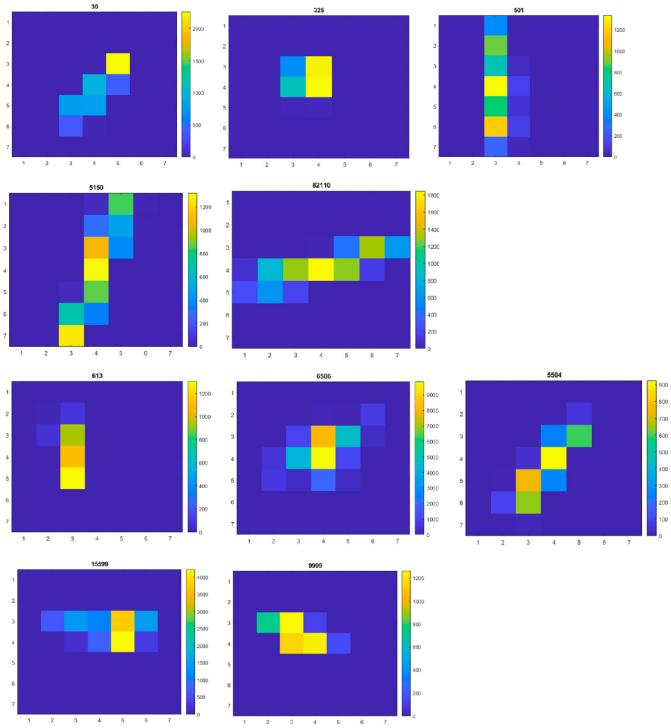

Fig. 6 Examples of cosmic rays from ESA library [7]

From several dark images taken by the EUCLID VIS instrument in flight, the CR rate observed was about 16 CRs per second per quadrant. For an FGS acquisition this results in 43 CRs per quadrant in case of 1.5 s of exposure time and 75 CRs per quadrant in case of 3.5 s of exposure time [7].

The results of the simulations are shown in Fig. 7, with the main observations summarized as follows [7]:

- The Cluster Filtering algorithm discards fewer than 6% of cosmic rays (CRs), as their energy and shape closely resemble stars, making them difficult for the algorithm to filter out.

- The double image filter effectively removes over 97% of CRs when the number of simulated CRs aligns with in-flight conditions (i.e., 300 CRs per texp = 3.5 s and 172 CRs per texp = 1.5 s). In the worst-case scenario, with 1500 CRs, the filter still performs well, discarding approximately 93% of the CRs.
- The double image filter successfully matches almost all simulated stars across all cases.

Through these simulations, LEONARDO demonstrated that the double image filter is highly effective at filtering out cosmic rays and matching stars.

Inputs						Results				
Texp [sec]	delta_T [sec]	Angular velocity [arcsec/sec]	Tollerance radius [pixels] = round(delta_T*Angular velocity/0.1)+4	Number of CRs in the FoV	Number of simulated stars	Number of matched stars	Number of matched CRs	% of discarded clusters by ALG-0060	% of discarded CRs by ALG-0061	% of matched stars
3.5	8	0.15	16	300	6	6	4	5.7	98.7	100.0
					25	25	3	5.2	99.0	100.0
					50	50	2	3.1	99.3	100.0
					400	397	3	1.9	99.0	99.3
3.5	8	0.22	22	300	6	6	4	4.8	98.7	100.0
					25	24	3	4.5	99.0	96.0
					50	50	8	3.9	97.3	100.0
					150	149	5	3.3	98.3	99.3
					400	397	8	1.8	97.3	99.3
				1500	150	148	109	4.8	92.7	98.7
1.5	6	0.3	22	172	6	6	1	4.4	99.4	100.0
					25	25	1	2.0	99.4	100.0
					50	49	2	5.3	98.8	98.0
					150	148	2	2.2	98.8	98.7
					400	398	3	1.7	98.3	99.5
				1500	150	147	103	4.8	93.1	98.0

Fig. 7 Double image correlator algorithm performance [7]

LEONARDO conducted additional simulations under in-flight conditions [7] to estimate a realistic worst-case performance. For Solar Maximum, 300 CRs were simulated within the CCD's FoV, while for Solar Minimum, 556 CRs were simulated per CCD FoV. During Solar Maximum, under the worst-case angular velocity of 0.22 arcsec/sec with a 3.5 second exposure time, more than 98% of CRs are discarded, and nearly all stars are successfully matched. During Solar Minimum, which represents the worst-case scenario for CR presence in the image, nearly all stars are matched, and with the worst-case angular velocity of 0.22 arcsec/sec, more than 96% of CRs are discarded.

All performed simulations by LEONARDO confirmed excellent capabilities of the double image filter to discard CRs and to match the stars.

5.2 Analysis of the reduced star signal measured in flight

During the FGS commissioning phase, an in-flight measurement revealed a lower-than-expected star signal compared to the onboard star catalogue [7]. Telemetry data from FGS indicated a total signal loss of approximately 0.76 magnitude.

An analysis [7] of raw pixel images acquired in-flight was conducted to assess the actual star signal captured by the CCD. This analysis showed a discrepancy of 0.36 magnitude between the computed star magnitude and the catalogue value, confirming that this portion of the signal loss is not due to FGS hardware.

The remaining 0.4 magnitude loss is attributed to the FGS star detection process, which relies on identifying pixels with signal levels above a predefined threshold. Any star signal below this threshold is not detected. When the overall star signal arriving at the CCD is lower, a larger portion of it falls below the threshold, compounding the measured loss. As a result, the reduced signal reaching the CCD has a dual impact: directly lowering the detected electrons and indirectly increasing the amount of undetected signal due to threshold limitations.

Considering the reduction of 0.36 magnitude of the signal arriving onto the CCD, ATM-AP simulations have been performed by LEONARDO [7] to evaluate the capability of FGS to solve the AP with a lower-than-expected star signal. For the simulations, a Point Spread Function (PSF) was provided by Thales Alenia Space Turin, having 30% of the energy in the central pixel for a best in-flight condition and 20% of energy in the worst condition. FGS image qualification in flight revealed that the magnitude offset cannot be explained by the FGS readout mode. The instrumental magnitude derivation from the GAIA Data Release 2 star catalogue compared with the FGS input star

catalogue has been entirely cross checked and compared with similar VIS instrument magnitudes and an error of less that 0.1 magnitude regarding to expectations could be assessed.
Therefore, the star catalogue generation process is found to be correct. The magnitude information is used by the FGS to perform pattern recognition and the applied threshold on this check is 1.0 magnitude. A pragmatic solution was found by lowering the reference star signal software parameter from 1.77E10 el/s to 9.29E9 el/s to recover the 0.7 magnitude difference. Fig. 8 shows the magnitude error of each individual PEC as a histogram derived from 50 different pointings from the 19th of September 2023. The Histograms confirm that the adopted reference star signal allowed a significant improvement of the measured magnitude.

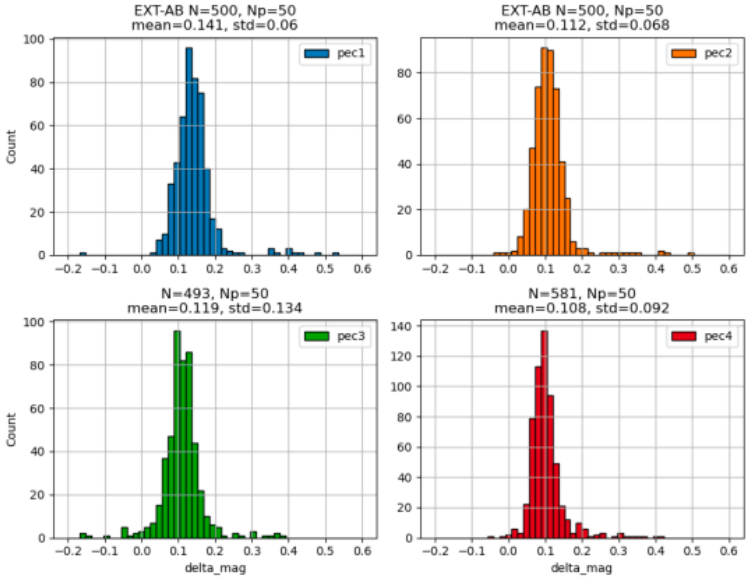

Fig. 8 Histograms of magnitude error after change of star reference signal

5. FGS re-commissioning after SW change

In early September 2023. LEONARDO delivered the new FGS ASW version 2.0.3.1, which included the double image correlator algorithm. TAS-I initially tested the software on the avionics model, still located in Turin at that time and confirmed with the initial test, that the new algorithm was working as expected. The upload of the new FGS ASW was conducted on the 18th of September 2023, starting with FGE EU1 for re-commissioning.

5.1 FGS stand alone functional verification

The scope of the first stand-alone functional verification tests was to verify the functionality of the two images over one low, one medium and one high star density field. For each star field two Photo Mode (PHM) image acquisitions (raw-pixel of the size 1000x600) were performed for each of the four quadrants of PEC L1 and PEC R1 on a medium star density field. After the raw pixel image acquisitions, the FGS was commanded into ATM-AP first with the algorithm disabled and then with the algorithm enabled to make a direct comparison of the FGS performance before versus after the SW modification. The same above was then repeated using PEC R2 and PEC L2. 4 different pointing attitudes were tested and in 100% of the cases the FGS resolved into ATM tracking phase with the updated SW.

5.2 High density star field

The sky density of the high density filed was about 400 stars per FoV with a star magnitude smaller than 18. The test verified that using the new SW, RTM, ATM-AP coarse and ATM-AP fine acquisitions were always performed using 10 tracked stars whereas the old SW showed a tracking performance with less stars. Fig. 9 shows the comparison of the possible target stars from the Input Star Catalogue versus the target stars found during ATM-AP.

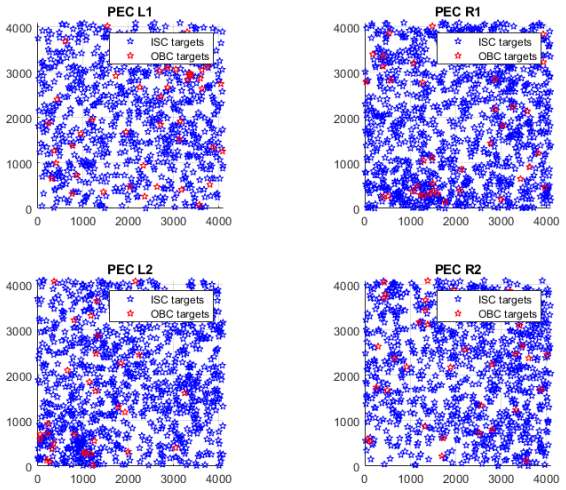

Fig. 9. OBC and ISC stars in High density sky field

5.3 Low density star field

The sky density of the low density filed was about 6 to 25 stars per FoV with a star magnitude smaller than 18. The test verified that using the new SW, RTM, ATM-AP coarse and ATM-AP fine acquisitions were always successful using between 6 to 10 tracked stars whereas with the old SW, RTM was able to track only 1 to 3 stars and ATM mode failed in all cases. Fig. 10 shows the comparison of the possible target stars from the Input Star Catalogue versus the target stars found during ATM-AP

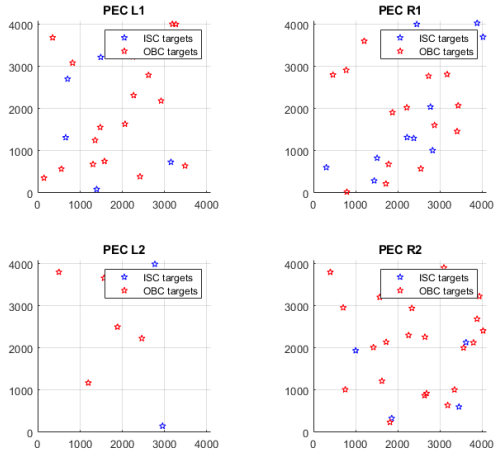

Fig. 10. OBC and ISC stars in low density sky field

5.4 Medium density star field

The sky density of the medium density filed was about 50 stars per FoV with a star magnitude smaller than 18. The test verified that using the new SW, RTM, ATM coarse mode and ATM fine acquisitions were always performed using 10 tracked stars, whereas with the old SW, RTM was able to track using 2 to 3 stars and ATM-TP was successful using 8 to 10 stars. Fig. 10 shows the comparison of the possible target stars from the Input Star Catalogue versus the target stars found during ATM-AP

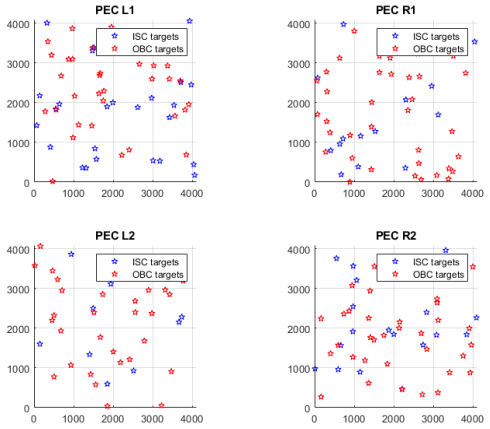

Fig. 11. OBC and ISC stars in low density sky field

5.5 Re-run of the FGS self-calibration fields

The test involved 50 different pointing attitudes at the north ecliptic pole, using the new SW with the double image correlator algorithm enabled and an exposure time of 3.5 seconds. Each pointing was separated by 400 arcseconds apart. The results showed that in 100% of the cases the FGS was able to perform successful attitude acquisition and transitioned into the Tracking phase. In contrast, with the old SW, the self-calibration performance achieved only a 50% success rate on the same sky field. Comparing Fig. 12 with Fig. 14 reveals that during the initial self-calibration with the original software, the FGS faced difficulties in the acquisition phase, resulting in either a complete acquisition failure or the system ending in relative tracking mode without utilizing the star catalogue. Additionally, the number of stars detected during the acquisition phase with the new software showed a marked improvement (see Fig. 13 and Fig. 15). A significantly larger number of stars were identified in the acquisition phase during the re-run of the self-calibration, and the number of stars tracked in ATM-TP was consistently higher compared to the previous self-calibration attempt.

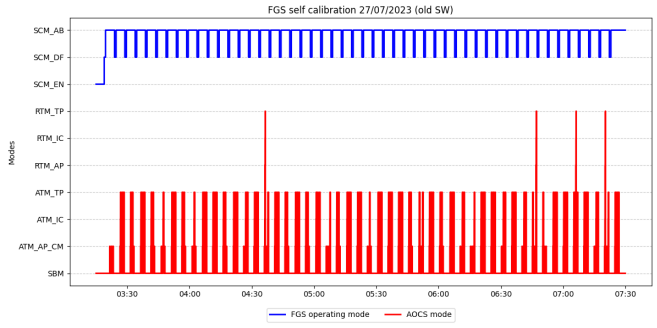

Fig. 12. AOCS and FGS operating modes during self calibration on 27/07/2023

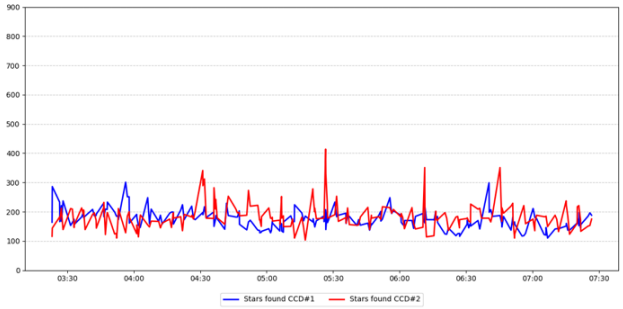

Fig. 13. Stars found during self-calibration on 27/07/2023

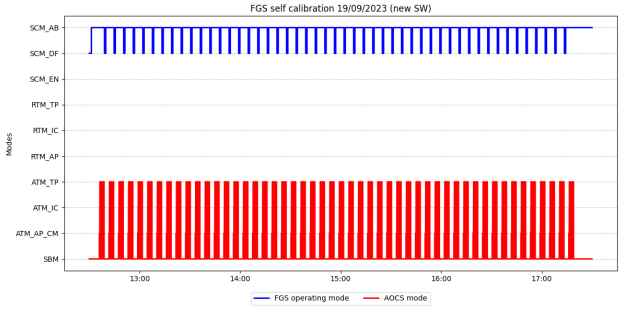

Fig. 14. AOCS and FGS operating modes during self calibration on 19/09/2023

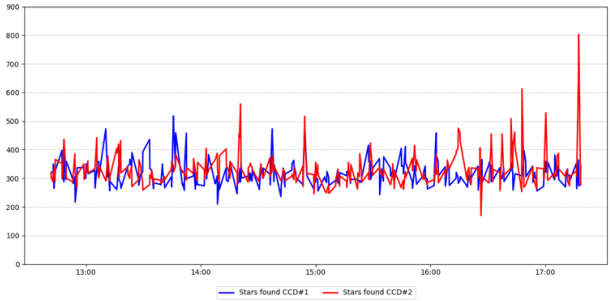

Fig. 15. Stars found during self-calibration on 19/09/2023

5.6 FGS robustness test over variety of different sky regions

After the self-calibration was successfully conducted, another 180 different attitude pointings were performed, where the spacecraft was slewed around the sun vector in 2 degrees increments (see Fig. 16).

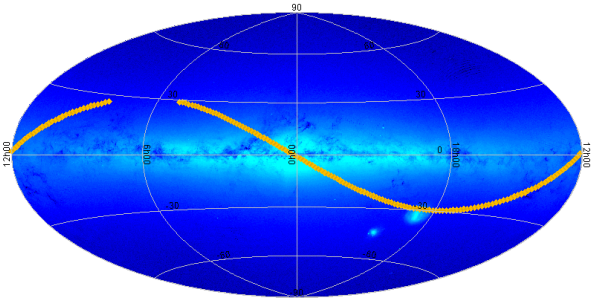

Fig. 16. Attitude pointings during FGS robustness test [6]

The sky star density varied from 30 to 3000 stars per FoV. The FGS was commanded on each pointing to achieve ATM-TP. Fig. 17 shows the star density of each PEC for each of the 180 attitude pointings. The OBC stars are the ones pre-selected by the On Ground Algorithm (OGA) tool and used by the FGS for tracking in each pointing. The OBC has a maximum amount of 80 stars per PEC per pointing.

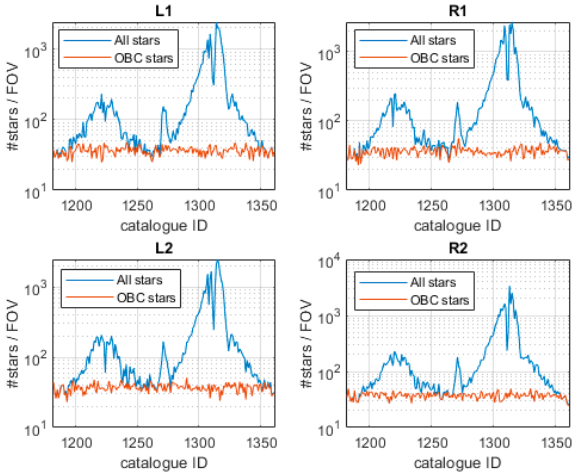

Fig. 17. Star density during FGS robustness test [6]

The test was run twice. In the initial run the FGS was not used in the AOCS control loop and the AOCS mode was SCM-AB. The second run was performed using the FGS for control and AOCS Mode was SCM_SO. Fig. 18 and Fig. 19 show the number of dropped objects versus the number of valid stars, which were found during each ATM-TP attempt. The dropped objects count is calculated by taking the total amount of stars found during ATM-TP and subtract this by the number of stars validated and matched with the on-board catalogue during ATM-TP. By comparing Fig. 18 with Fig. 20 in can be seen, that in all sky densities the FGS found enough stars to perform successful tracking. The same applies for Fig. 19 and Fig. 21.

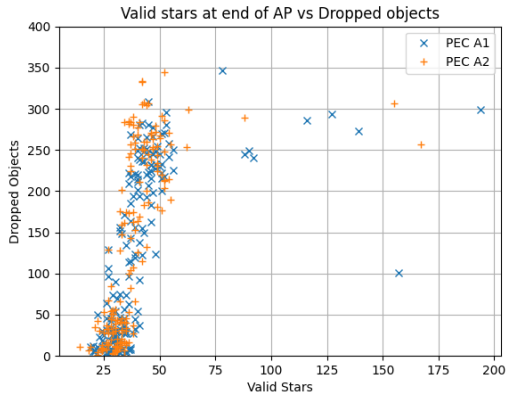

Fig. 18. Valid stars at end of AP versus dropped objects during FGS robustness test in SCM_AB

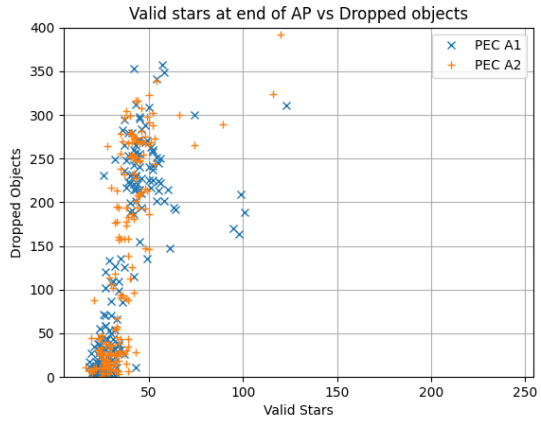

Fig. 19. Valid stars at end of AP versus dropped objects during FGS robustness test in SCM_SO

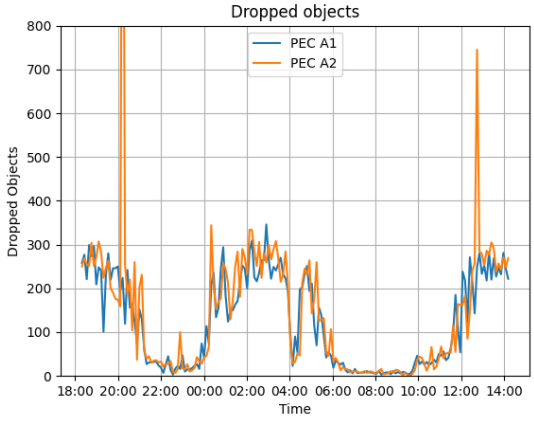

Fig. 20. Dropped objects during FGS robustness test in SCM_AB

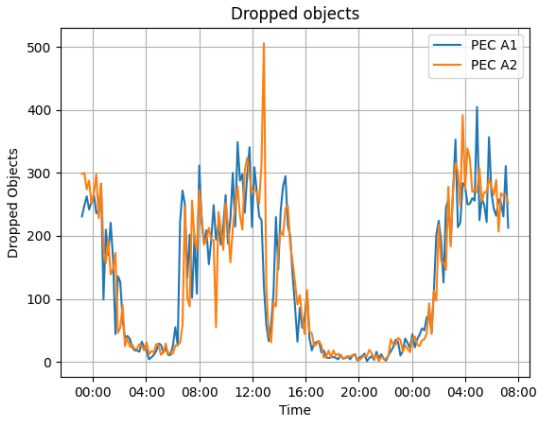

Fig. 21. Dropped objects during FGS robustness test in SCM_SO

6. Conclusions

The implementation of the FGS double image correlator algorithm during the ATM-AP/RTM-AP was a complete success, addressing the issues encountered during the first FGS commissioning campaign. The paper presented simulations of the algorithm, demonstrating that the robustness test results were consistent with the ground predictions. The reduced probability of success in the AP was mitigated by the presence of a large number of cosmic rays, which were superimposed on a weak star field due to star signal loss. This weakened the FGS's ability to detect dimmer stars and match star triads [7]. However, with the new FGS ASW 2.0.3.1, the acquisition phase was successfully completed, and tracking was initiated for all pointing and CCD pairs. As a result, ASW 2.0.3.1 achieved 100% success in solving the AP, compared to only 50% success with the previous ASW version under the same sky conditions. This confirms that the double image correlator implementation in AP, along with the increase in exposure time, resolved all FSG commissioning issues. Additionally, the RTM AP was enhanced by the introduction of the double image filter, which prevents the selection of cosmic rays as stars to track, thereby reducing the risk of failure in both the intermediate and subsequent tracking cycles.

Acknowledgements

The author would like to thank TAS-I and LEONARDO for the excellent work provided to get a new FGS ASW operational in such a short time and help EUCLID starting with the performance verification phase.

References

[1] G. Racca, The Euclid mission design, https://arxiv.org/abs/1610.05508.
[2] Euclid Collaboration: Y. Mellier, Euclid. I. Overview of the Euclid, 25 September 2024, https://arxiv.org/pdf/2405.13491
[3] C. Finocchietti, FGS Design Report, Euclid Collaboration Document, EUCL-SES-RP-2-003 version 8, 23 December 2021
[4] C. Ostorero, In Flight System Performance Verification and Calibration Plan, Euclid Collaboration Document, EUCL-TAST-PL-1-028 version 6, 31 January 2023
[5] A. Perna, FGS General Design Description, Euclid Collaboration Document, EUCL-SES-TN-2-016 version 1, 23 February 2018
[6] Thales Alenia Space Italy, Commissioning report for MCRR, Euclid Collaboration Document, EUCL-TAST-PRS-1-0021 version 1, 11 November 2023
[7] C. Finocchietti, FGS In-Flight Commissioning Report, Euclid Collaboration Document, EUCL-SES-TR-2-066 version 1, 2 November 2023